ACS Chemical Neuroscience

Article

Label-Free Electrochemical Biosensor for Monitoring of Chloride Ion in an Animal Model of Alzhemier's Disease

Hui Dong, Limin Zhang, Wei Liu, and Yang Tian

ACS Chem. Neurosci., **Just Accepted Manuscript** • DOI: 10.1021/acschemneuro.6b00296 • Publication Date (Web): 06 Dec 2016

ACS Publications

ACS Chemical Neuroscience is published by the American Chemical Society. 1155 Sixteenth Street N.W., Washington, DC 20036

Label-Free Electrochemical Biosensor for Monitoring of Chloride Ion in an Animal Model of Alzhemier's Disease

Hui Dong, Limin Zhang, Wei Liu, Yang Tian*

Shanghai Key Laboratory of Green Chemistry and Chemical Processes, Department of Chemistry, School of Chemistry and Molecular Engineering, East China Normal University, Dongchuan Road 500, Shanghai 200241, China.

Corresponding author.

*E-mail: ytian@chem.ecnu.edu.cn; Fax: +86-21-54341041.

ABSTRACT:

The potential damage of Alzheimer's disease (AD) in brain function has attracted extensive attentions. As the most common anion, Cl^-, has been indicated to play significant roles in brain diseases, particularly in pathological process of AD. In this work, a label-free selective and accurate electrochemical biosensor was first developed for real-time monitoring of Cl^- levels in mouse brain model of AD and rat brain upon global cerebral ischemia. Silver nanoparticles (AgNPs) were designed and synthesized as selective recognition element Cl^-, while 5'-MB-GGCGCGATTTT-SH-3' (SH-DNA-MB, MB = methylene blue), was selected as an inner reference molecule for a built-in correction to avoid the effects from the complicated brain. The electrochemical biosensor showed high accuracy and remarkable selectivity for determination of Cl^- over other anions, metal ions, amino acids, and other biomolecules. Furthermore, three dimensional nanostructures composing of single-walled carbon nanotubes (SWNT) and Au nanoleaves were assembled on the carbon fiber microelectrode (CFME) surface to enhance the response signal. Finally, the developed biosensor with high analytical performance, as well as unique characteristic of CFME itself including easy to inert in live brain and good biocompatibility, was successfully applied to in vivo determination of Cl^- levels in three brain regions: striatum, hippocampus, and cortex of live mouse and rat brains. The comparison of average levels of Cl^- in normal striatum, hippocampus, and cortex of normal mouse brains and those in the mouse model brains of AD was reported. In addition, the results in the rat brains followed by cerebral ischemia demonstrated that the concentrations of Cl^- decreased by $19.8 \pm 0.5\%$ ($n = 5$) in the striatum and $27.2 \pm 0.3\%$ ($n = 5$) in hippocampus of rat brains after cerebral ischemia for 30 min, but negligible change in Cl^- concentration was observed in cortex.

KEYWORDS: *Chloride ion, Silver Nanoparticles, Electrochemical Biosensors, Alzheimer's disease, Cerebral ischemia*

INTRODUCTION

With aging of world population and increasing life expectancy, as one of progressive neurodegenerative diseases, Alzhemier's disease (AD) affects millions of people every year, and has become a severe social and economic problem in modern societies. The AD brain is characterized by the presence of intraneuronal neurofibrillary tangles constituted by the hyperphosphorilated form of the cytoskeleton protein Tau and deposites of the amyloid beta (Aβ) protein, also known as senile plaques.[1-4] As one of the anion channels, chloride ion (Cl^-) channel which plays the critical roles in the physiology of neurons related to AD have been extensively studied.[5-12] It is widely believed that the inflammatory events mediated by microglial activation contribute to several neurodegenerative processes, including AD. Activation of microglia by Aβ peptides results in an overall increase in chloride intracellular channel-1 (CLIC1) protein with resultant increase in CLIC1 ion channel activity, suggesting the close relationship between Cl^- and brain diseases. Furthermore, in amyloid-b (Ab)-stimulated microglial cells, blockade of CLIC1 reverts the increase in tumor necrosis factor and nitric oxide production and results in neuroprotection of cocultured neurons. This effect could be of therapeutic efficacy in AD, where microglial activation may contribute to neurodegeneration, but it could reduce Ab phagocytosis, which could facilitate amyloid plaque removal.[12] However, the clear mechanism is still unknown at the present stage. Thus, it is pressing to firstly develop a selective and accurate tool for in vivo determination of Cl^- in live brain, and further for understanding the signal pathway of Cl^- plays in the brain diseases, as well as for therapy.

To date, a large amount of methods have been reported for detection of Cl^-, such as turbidimetry,[13] liquid chromatography,[14] fluorescence,[15-19] and electrochemical methods.[20-25] In contract to the other methods, electrochemical strategy shows remarkable advantages in high temporal and spatial resolution, easy miniaturization, as well as real-time and in vivo measurements in live animals.[26-36] Although Cl^- ion-selective electrodes have been widely utilized for determination of Cl^- in biofluid and environmental samples,[37-40] it is still a great challenge to create an accurate biosensor applicable for real-time detection of Cl^- directly in live brain. Herein, a label-free electrochemical biosensor was developed with inner reference element for in vivo monitoring of Cl^- levels in a mouse model of AD, as well as in rat brain upon cerebral ischemia (Scheme 1). First of all, silver nanoparticle (AgNP) was designed and synthesized as a selective recognition element to detect Cl^-, over potential

interferences such as other anions, metal ions, amino acids, reactive oxygen and nitrogen species (ROS/RNS), and other biological species. The oxidation peak potential of AgNPs shifted with increasing concentration of Cl^- because of chemical reaction between AgNPs and Cl^- to generate AgCl precipitate, resulting in a wide linear range for Cl^- determination from 1 mM to 300 mM according to the Nernst equation. Meanwhile, methylene blue (MB)-labeled oligonucleotide (SH-DNA-MB) with well-separated oxidation peak from AgNPs was optimized as an inner reference element for providing a built-in correction to avoid the determination error due to the distinct environments between in vitro and in vivo. Such a Cl^- biosensor using potential difference between oxidation peak potentials of AgNPs and SH-DNA-MB effectively improved the accuracy for Cl^- measurement in complicated brain. Furthermore, three dimensional nanostructures composing of carbon nanotubes and gold nanoleaves were assembled on carbon fiber microelectrode (CFME), remarkably enhanced the current response. Eventually, the developed biosensor for Cl^- with high analytical performance, as well as the unique properties of CFME including small size down to 10 μm and good biocompatibility,[29-36, 41] was realized a direct and reliable determination of Cl^- in a mouse model of AD and rat brain upon ischemia. We found that the concentration of Cl^- decreased clearly in hippocampus, but no obvious changes were obtained in cortex and striatum in the mouse model of AD, compared to those in normal mouse brain. In addition, the concentrations of Cl^- also obviously went down in hippocampus and striatum after cerebral ischemia for 30 min, while negligible change was observed in cortex. To the best of our knowledge, these results have never been reported.

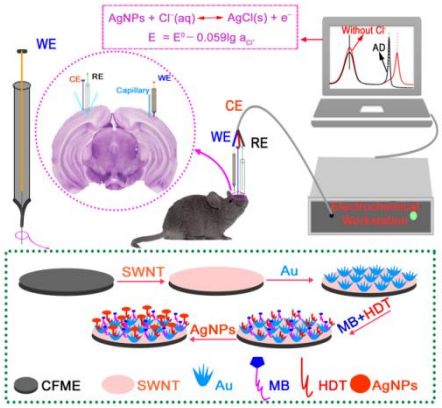

Scheme 1. The developed electrochemical biosensor for in vivo monitoring of Cl^- in a live mouse brain.

RESULTS AND DISCUSSION

First of all, AgNPs were synthesized according to previous literature.[42] UV-Vis spectroscopy was utilized to verify the formation of AgNPs from $AgNO_3$ solution (Figure S1, Supporting Information). A typical absorption peak observed at 395 nm implied generation of AgNPs.[43, 44] From transmission electron microscopic (TEM) image shown in Figure 1A, we can see well-dispersed AgNPs were clearly observed with uniform sphere nanostructure, and the histogram (Figure 1B) showed that the average size of the AgNPs was 5.2 ± 0.5 nm (n = 100). Furthermore, as shown in Figure 1C, the clear lattice fringes with a distance of 0.24 nm is compatible with [111] planes of Ag, confirming successful synthesis of AgNPs.[45]

On the other hand, single walled carbon nanotubes (SWNTs) with averaged diameter of 20 nm shown in Figure S2A (Supporting Information), were densely covered on bare CFME surface through π-π stacking. This electrode was denoted as CFME/SWNT. Then, three-dimensional Au nanoleaves were further electrodeposited on CFME/SWNT surface, in 5 mM $HAuCl_4$ at an applied potential of - 0.2 V, to obtain CFME/SWNT/Au electrode (Figure S2B, Supporting Information). From a close observation for Au nanoleaves, we can see that the length of Au nanoleaves was ~ 2 μm on average (Figure S2C, Supporting Information). From X-ray photoelectron spectroscopic

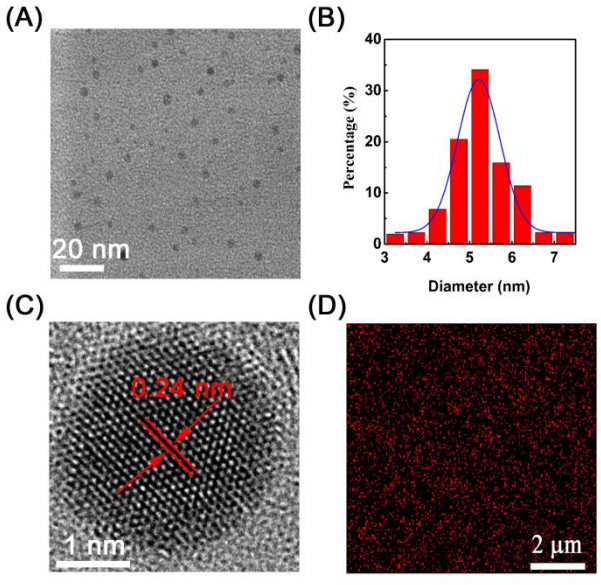

Figure 1. (A) TEM image, (B) Diameter distribution, (C) HRTEM, and (D) EDX analysis of AgNPs.

(XPS) data, two peaks of Au $4f_{5/2}$ at 87.7 eV, and Au $4f_{7/2}$ at 84.0 eV were observed clearly in Figure S3A (curves b-d, Supporting Information), while no peak was obtained from CFME/SWNT

(curve a, Supporting Information). The results indicated that Au nanoleaves were composed of ploycrystalline gold. Followed by that, SH-DNA-MB and 1,6-hexanedithiol (HDT) were simultaneously assembled onto CFME/SWNT/Au electrode through Au-S bond. The as-prepared electrode was denoted as CFME/SWNT/Au/MB+HDT hereafter. The modification processes were tracked by XPS. As shown in Figure S3B (Supporting Information), a P $2p_{3/2}$ peak was observed at 134.3 eV, demonstrating that SH-DNA-MB was assembled on the CFME/SWNT/Au. Meanwhile, two peaks of S $2p_{3/2}$ (163.6 eV) and S $2p_{1/2}$ (162.3 eV) were obtained in curve c of Figure S3C (Supporting Information), which were ascribed to unbound alkanethiols and self-assembled thiol groups of MB and HDT on Au surface, respectively. After AgNPs were confined on CFME/SWNT/Au/MB+HDT surface, the intensity of S $2p_{3/2}$ peak at 163.6 apparently decreased, demonstrating the unbound thiols of HDT reacted with AgNPs. The assembly of AgNPs was further evident by two peaks of Ag $3d_{3/2}$ at 374.6 eV and Ag $3d_{5/2}$ 368.5 eV observed in curve d of Figure S3D (Supporting Information). The AgNPs-assembled electrode was denoted as CFME/SWNT/Au/MB+HDT/AgNPs. The energy dispersive X-ray spectroscopy (EDX) analysis (Figure 1D and Figure S2D, Supporting Information) also confirmed Ag element was uniformly distributed on the electrode surface.

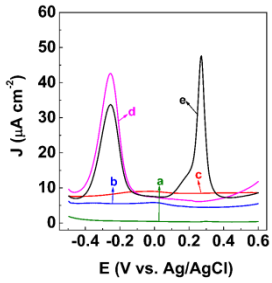

Figure 2. DPVs obtained at (a) CFME, (b) CFME/SWNT, (c) CFME/SWNT/Au, (d) CFME/SWNT/Au/MB+HDT, and (e) CFME/SWNT/Au/MB+HDT/AgNPs electrodes in 0.1 M PBS (pH 7.4).

Then, electrochemical characterization was carried out using differential pulse voltammetry (DPV). As displayed in Figure 2A, only one anodic peak located at - 0.25 V vs. Ag/AgCl was obtained at CFME/SWNT/Au/MB+HDT in 0.1 M PBS solution (pH 7.4) (curve d), while no anodic peak was observed at bare CFME (curve a), CFME/SWNT (curve b), and CFME/SWNT/Au (curve c). Thus, such an anodic peak was attributed to oxidation of MB on the electrode surface.[46] After

AgNPs were assembled on the electrode surface of CFME/SWNT/Au/MB+HDT (curve e), another narrow anodic peak was clearly obtained at ~ 0.27 V which was well-separated from that of MB was obtained. Furthermore, both anodic peak currents of MB and AgNPs showed a good linear relationship with increasing scan rates in the range of 60-420 mV s^{-1}, indicating the oxidation of MB and AgNPs are surface-controlled processes (Figure S4, Supporting Information). This peak observed at 0.27 V was ascribed to oxidation of AgNPs on CFME/SWNT/Au/MB+HDT electrode surface as expressed by Reaction (1). When Cl^- was added into the solution, a subsequent chemical Reaction (2) follows Reaction (1). This whole process is summarized as Reaction (3).[47] On the basis of Nernst equation, the relationship between $E_{Ag+/Ag}$ and Cl^- concentration can be expressed by Equation (1). According to Equation (1), it can be seen that the $E_{Ag+/Ag}$ value is linearly dependent on the logarithm of Cl^- concentration, and decreases with increasing concentration of Cl^-. Such relationship between $E_{Ag+/Ag}$ and Cl^- concentration establishes the theoretical basis for Cl^- determination.

$$Ag\ (s) \rightarrow Ag^+\ (aq) + e^- \qquad \text{(Reaction 1)}$$

$$Ag^+ + Cl^- \rightarrow AgCl \qquad \text{(Reaction 2)}$$

$$Ag\ (s) + Cl^-\ (aq) \rightarrow AgCl\ (s) + e^- \qquad \text{(Reaction 3)}$$

$$E_{Ag^+/Ag} = E^0_{AgCl/Ag} - 0.0591 \lg c_{Cl^-} \qquad \text{(Equation 1)}$$

Next, DPVs of CFME/SWNT/Au/MB+HDT/AgNPs electrode were recorded in 0.1 M PBS (pH 7.4) with different concentrations of Cl^-. As demonstrated in Figure 3A, oxidative peak potential of AgNPs (E_p(Ag)) at 0.27 V was Cl^- concentration-dependent, shifting negatively with increasing concentrations of Cl^-. However, oxidative peak potential of MB (E_p(MB)) located at - 0.25 V remained almost constant with the changes of Cl^- concentration, resulting in accurate determination of Cl^- concentration with inner reference. The separation between E_p(Ag) and E_p(MB) ($\Delta E_p = E_p$(Ag) - E_p(MB)) exhibited a good linearity with the logarithm of Cl^- concentration in the range from 1 mM to 300 mM with a detection limit of 10 μM. The calibration plot of ΔE_p against Cl^- concentration showed a gradient of - 58.3 mV $decade^{-1}$ (Figure 3B). This gradient is close to the theoretically value calculated from Equation (1). The current signals for MB and Ag obtained at CFME/SWNT/Au/MB+HDT/AgNPs were estimated to be 2-fold greater than that obtained at Au/MB+HDT/AgNPs due to the large surface area of nanocomposites of SWNT and Au nanoleaves

(Figure S5, Supporting Information).[32, 34, 48]

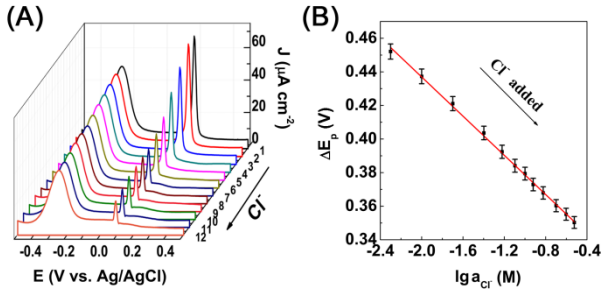

Figure 3. (A) DPVs obtained at CFME/SWNT/Au/MB+HDT/AgNPs electrode in 0.1 M PBS (pH 7.4) with different concentrations of Cl^- (they are 1, 5, 10, 20, 40, 60, 80, 100, 150, 200, 250, 300 mM from 1 to 12, respectively). (B) The linear relationship of ΔE_p against the logarithm of Cl^- concentrations in the range of 1 to 300 mM. Each point represents the mean ± standard deviation (SD) of five independent experiments.

As demonstrated above, the developed potentiometric biosensor exhibited remarkable analytical performance such as high sensitivity and accuracy for determination of Cl^-. However, it is still a great challenge for selective detection in the complicated brain system. The selectivity of the present CFME/SWNT/Au/MB+HDT/AgNPs was evaluated by determination of $(\Delta E_p^0-\Delta E_{p(I)})/\Delta E_p^0$ values in 0.1 M PBS (pH 7.4) originating from other potential interferences, in which ΔE_p^0 represents ΔE_p value after addition of 100 mM Cl^- according to the real level of Cl^- in brain,[49] and $\Delta E_{p(I)}$ is ΔE_p value after addition of others interferences. The concentrations of interferences were almost determined by the real concentrations reported in rat brain.[32, 33, 36, 50-54] The interferences from anions (F^-, SO_4^{2-}, CO_3^{2-}, OH^-, Ac^-, NO_3^-, HPO_4^{2-}, ClO_4^-, Br^-, I^-) were firstly considered, particularly for Br^- and I^-, because they can also react with Ag to form the precipitation, and then trigger the shift of E_p(Ag), resulting in the potential interferences towards Cl^- determination. In fact, E_p(Ag) is theoretically related to solubility product (K_{sp}) of Ag complex. Thus, different K_{sp} values obtained for complexes of AgCl (1.8×10^{-10}), AgBr (5.0×10^{-13}), and AgI (8.3×10^{-17}) would make E_p(Ag) shift to different potential with the same concentration. As shown in curve a of Figure S6A-C (Supporting Information), in the blank PBS solution, E_p(Ag) was observed at 0.27 V. However, E_p(Ag) values shifted to 0.22 V for AgCl, 0.09 V for AgBr, and - 0.10 V for AgI, after 1 mM Cl^-, Br^-, and I^- were added into the blank PBS (Curve b of Figure S6A-C, Supporting Information), respectively. The

E_p(MB) remained constant. These results demonstrated that the determined peak potential for Cl^- cannot be interfered by Br^- and I^- even if three anions Cl^-, Br^-, and I^- were coexisted in solution with same concentration, as confirmed by Figure S6D (Supporting Information). Three well-separated anodic peaks were observed at 0.22 V, 0.09 V, and -0.10 V vs. Ag/AgCl, which were attributed to the oxidation peaks of AgCl, AgBr, and AgI, respectively (Curve b of Figure S6D, Supporting Information), and almost no potential shift (< 5%, n = 5) was obtained (as shown in Figure 4A) upon addition of others anions, indicating no interference was obtained for all potential anions against Cl^- determination.

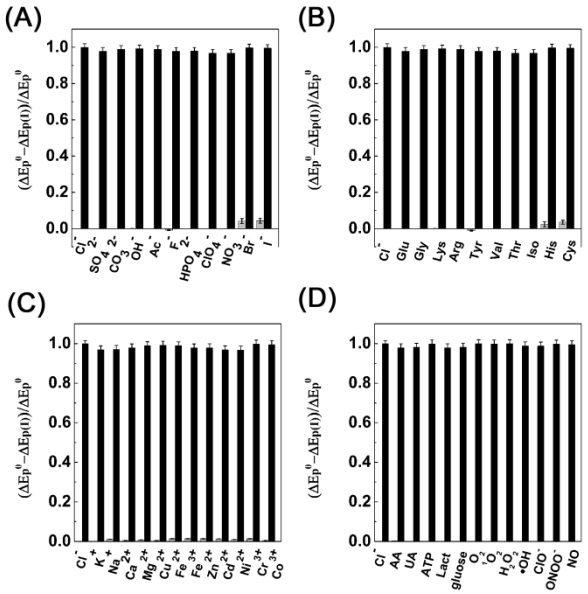

Figure 4. Selectivity and competition tests of (A) anions against Cl^-, from left to right: (1) Cl^-, (2) SO_4^{2-}, (3) CO_3^{2-}, (4) OH^-, (5) Ac^-, (6) F^-, (7) HPO_4^{2-}, (8) ClO_4^-, (9) NO_3^-, (10) Br^-, and (11) I^- (1 mM for 6, 10 and 11, 10 μM for others), (B) amino acids against Cl^-, from left to right: (1) Cl^-, (2) Glu, (3) Gly, (4) Lys, (5) Arg, (6) Try, (7) Val, (8) Thr, (9) Iso, (10) His, and (11) Cys (5 μM for 2 to 11), (C) cations against Cl^-, from left to right: (1) Cl^-, (2) K^+, (3) Na^+, (4) Ca^{2+}, (5) Mg^{2+}, (6) Cu^{2+}, (7) Fe^{2+}, (8) Fe^{3+}, (9) Zn^{2+}, (10) Cd^{2+}, (11) Ni^{2+}, (12) Cr^{3+}, and (13) Co^{3+} (50 mM for 2, 100 mM for 3, 1 mM for 4 to 5, 5 μM for 6 to 13), (D) ROS/RNS and other biomolecules against Cl^-, from left to right: (1) Cl^-, (2) AA , (3) UA, (4) ATP, (5) Lac, (6) Glucose, (7) O_2, (8) $^1O_2$, (9) H_2O_2, (10) •OH, (11) ClO^-, (12) $ONOO^-$, and (13) NO (300 μM for 2, 1 mM for 6, other species are 5 μM). Error bar represents the means ± SD values from five independent experiments.

In addition, the interferences included metal (K^+, Na^+, Ca^{2+}, Mg^{2+}, Cu^{2+}, Fe^{2+}, Fe^{3+}, Zn^{2+}, Cd^{2+}, Ni^{2+}, Cr^{3+}, Co^{3+}), amino acids (Cys, Glu, Gly, His, Lys, Iso, Arg, Try, Val, Thr), ROS/RNS (O_2, $^1O_2$,

H_2O_2, •OH, ClO^-, and $ONOO^-$), and other biological species (ascorbic acid (AA), dopamine (DA), adenosine triphosphate (ATP), glucose, uric acid (UA), lactic acid (Lac)), were also tested. As shown in Figure 4B-D, slight potential shift (< 5.0%, n = 5) was obtained upon the addition of metal ions, amino acids, ROS/RNS, and other biological species. Moreover, negligible changes (< 4.2%, n = 5) were observed for competition test. These results demonstrated the present CFME/SWNT/Au/MB+HDT/AgNPs possessed high selectivity for determination of Cl^- over other anions, metal ions, amino acids, ROS/RNS and other biological species, which can fulfill the requirement for selectivity of in vivo analysis.

Furthermore, reproducibility of the present sensor was tested for further application in animal brains. Five different CFME/SWNT/Au/MB+HDT/AgNPs electrodes were tested in 0.1 M PBS (pH 7.4) containing Cl^- with the concentrations ranging from 1 to 300 mM. The relative standard deviation (RSD) was smaller than 3.5% (n = 5) (Figure S7, Supporting Information), demonstrating good reproducibility of the developed electrode. More importantly, the anodic peak potentials of AgNPs and MB shifted no exceeded 0.8% even after consecutive potential scanning for 100 cycles, revealing a high scanning stability (Figure S8A, Supporting Information). In addition, negligible change (< 4.1%, n = 5) in DPV responses obtained at CFME/SWNT/Au/MB+HDT/AgNPs before (curve a) and after being stored at 4°C for 15 days (curve b of Figure S8B, Supporting Information) indicated that the present biosensor for Cl^- possessed long-term stability. Such excellent stability was relatively important for further application in the complicated brain environment.

As demonstrated above, the developed electrochemical biosensor for Cl^- demonstrated remarkable analytical performance including high selectivity and accuracy, long-term stability, as well as good reproducibility. Combined with microelectrode technique, the present biosensor was utilized for in vivo monitoring of Cl^- levels (APPswe/PS1dE9 transgenic mouse of AD was employed as a mouse model of AD; adult male Wistar rat was employed for cerebral ischemia experiments). As shown in Figure 5A, two separated oxidation peaks were clearly observed at - 0.25 V and 0.15 V at CFME/SWNT/Au/MB+HDT/AgNPs in the hippocampus of normal mouse brain. The basal level of Cl^- in the normal mouse brains were estimated to be 56 ±4 mM (n = 5) in striatum, 57 ±3 mM (n = 5) in cortex, and 100 ±5 mM (n = 5), in hippocampus, respectively. However, in the mouse brain model of AD, as given in curve b shown in Figure 5A (and enlarged Figure 5B), oxidation peak of AgNPs shifted positively, corresponding to the decrease of Cl^- concentration down

to 64 ±3 mM (n = 5) in hippocampus. However, the levels of Cl^- in striatum and cortex showed no obvious changes. This newly developed methods was further compared with the traditional Volhard's method[55] for determination Cl^- in hippocampus microdialysates of normal mouse brain and the mouse brain model of AD (Table S1, Supporting Information). According to the statistic calculation by a t test (P = 0.05, n = 3), the concentrations of Cl^- determined by the present method coincided well with those by Volhard's method (t = 1.16 for normal mouse, t = 0.31 for mouse brain model of AD, which were smaller than the standard t value of 2.78 (P = 0.05, n = 3), which confirmed the accuracy of the present sensor for Cl^- determination. However, the standard Volhard's method can only be used in determination of Cl^- in microdialysates because it needs to titrate $AgNO_3$ and $NH_4Fe(SO_4)_2$ into sample, which is unavailable to in vivo determination in brain. Superior to standard Volhard's method, the present developed biosensor can not only determine the Cl^- levels in microdialysates, but also can directly monitor Cl^- in live brain.

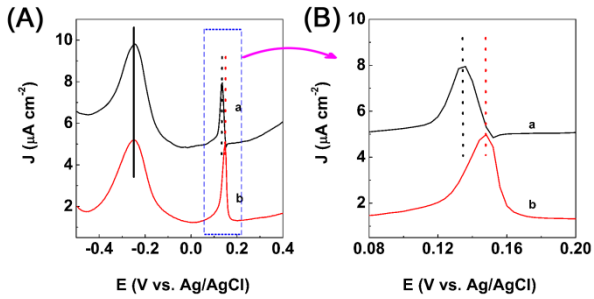

Figure 5. (A) DPV responses obtained at CFME/SWNT/Au/MB+HDT/AgNPs electrodes for determination of Cl^- in the hippocampus of (a) normal mouse brain and (b) a mouse brain model of AD. (B) The enlarged view of labelled area in Figure 5(A).

We also applied the developed electrochemical biosensor for real-time monitoring of Cl^- levels in three brain regions at different times following by global cerebral ischemia (Figure 6). The results indicated that the concentration of Cl^- decreased by 19.8 ± 0.5% (n = 5) in the striatum and 27.2 ± 0.3% (n = 5) in the hippocampus within 30 min. This phenomenon might be explained by the activation of Cl^-/HCO_3^- exchanger or $Na^+/K^+/Cl^-$ co-transporter (NKCC1).[56, 57] On one hand, the occurrence of cerebral ischemia would trigger the accumulation of extracellular γ-aminobutyric acid (GABA) in striatum and hippocampus, resulting in influx of Cl^- and efflux of HCO_3^- through GABA-gated Cl^- channel.[56] On the other hand, the cerebral ischemia would lead to increase NKCC1

protein expression in striatum and hippocampus, consequently makes Cl^- concentration in cerebrospinal fluid decrease.[57] However, negligible change in Cl^- concentration was observed in the cortex region upon cerebral ischemia. Such distinction may be explained by weak cerebral ischemia in cortex through compensation from vertebral artery. Because the cerebral ischemia surgery in our investigation was performed just by carotid artery ligation. Once cerebral ischemia occurred, rich vascular networks formed by superficial branch would help the blood flow of vertebral artery supplied to cortex sufficiently through collateral circulation, resulting in Cl^- concentration hardly affected by cerebral ischemia through carotid artery ligation.[58-61] In contrast, hippocampus and striatum contain many terminal arteries, and then the blood flow cannot be supplied through vertebral artery.[60, 61] Therefore, obvious cerebral ischemia triggered obvious decrease of Cl^- concentration.

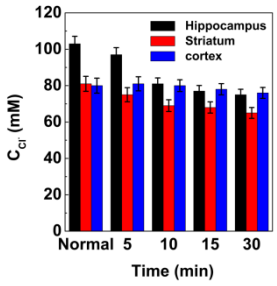

Figure 6. The levels Cl^- determined in three regions of rat brains before and after global cerebral ischemia with different time. Bars represent the means ± SD values from five different animals.

CONCLUSION

In summary, we developed an accurate and selective electrochemical biosensor for determination of Cl^- levels in live brains, in which AgNPs were designed as selective recognition element for Cl^- and SH-DNA-MB was synthesized as inner reference element. The developed biosensor showed high accuracy and remarkable selectivity for Cl^- determination against other anions, metal ions, amino acids, ROS/RNS, and other biological species. The good reproducibility and long-termed stability of the present biosensor made it very powerful for further application in three regions: striatum, hippocampus, and cortex of live mouse and rat brains. The basal level of Cl^- in the normal mouse brains were estimated to be 56 ± 5 mM (n = 5) in striatum, 57 ± 3 mM (n = 5) in cortex, and

100 ± 5 mM (n = 5) in hippocampus on average, respectively. However, in the mouse brain model of AD, the Cl^- concentration decreased to 64 ± 3 mM (n = 5) in hippocampus, the levels of Cl^- in striatum and cortex showed no obvious changes. Meanwhile, the concentrations of Cl^- decreased by 19.8 ± 0.5% (n = 5) in the striatum and 27.2 ± 0.3% (n = 5) in hippocampus of rat brains after cerebral ischemia for 30 min, but negligible change in Cl^- concentration was observed in cortex. The information should be very valuable for understanding the roles that Cl^- plays in the physiological and pathological processes of brain, as well as for developing the therapeuric drugs for brain diseases. More importantly, this work can be extended to design and construct high-performance biosensors for other anions, and may encourage new directions in brain chemistry research.

METHODS

Chemicals. Silver nitrate ($AgNO_3$) was obtained from Sinopharm Chemical Reagent Co. Ltd. (Shanghai, China). Sodium borohydride ($NaBH_4$), 1,6-hexanedithiol (HDT), trisodium citrate (TSC), chloroauric acid trihydrate ($HAuCl_4 \cdot 3H_2O$), ascorbic acid (AA), dopamine (DA), adenosine triphosphate (ATP), glucose, uric acid (UA), lactic acid (Lact), H_2O_2, KO_2, S-nitroso-N-acetyl-DLpenicillamine (SNAP), 4,4'-diisothiocyanostilbene-2,2'-disulfonic acid (DIDS), and all amino acids were purchased from Sigma-Aldrich (USA). Oligonucleotide, 5'-MB-GGCGCGATTTT-SH-3' (SH-DNA-MB), was synthesized by TaKaRa Biotechnology Co. Ltd. (Dalian, China). SWNTs (<2 nm in diameter and 0.5-50 μm in length) were purchased from Shenzhen Nanotech Co. Ltd. (Shenzhen, China) and used without further purification. All other chemicals and reagents were analytical grade, and directly used without further purification.

Different reactive oxygen and nitrogen species (ROS/RNS) were produced as follows: SNAP (1 mM) was dissolved in 0.1 M phosphate buffer (pH 7.4) to produced nitric oxide (NO). Peroxynitrite ($ONOO^-$) solution was provided by KNO_2 (0.6 M) and H_2O_2 (0.7 M) in hydrochloric acid (0.6 M) at 0 °C and was stored at - 20°C. KO_2 was performed to generate $O_2^{\bullet-}$ in the DMSO. Singlet oxygen ($^1O_2$) was generated based on the reaction of H_2O_2 and NaClO (H_2O_2: NaClO = 1:1). •OH was generated from the Fenton reaction of ferrous ammonium sulfate with H_2O_2 (Fe^{2+}: H_2O_2 = 1 : 6). All aqueous solutions were prepared with ultrapure water (18.2 MΩ cm^{-1}), supplied by a millipore M-Q purification system.

Synthesis of AgNPs. Silver nanoparticles (AgNPs) were synthesized as previously reported.[42] Briefly, $AgNO_3$ (0.0102 g) and TSC (0.0141 g) were firstly dissolved in deionized water (200 ml) under vigorous stirring in dark environment and the solution was kept in an ice bath. Then, $NaBH_4$ aqueous solution (0.1 M) was quickly added and the mixed solution was further stirred for 1 h into a yellow suspension. Finally, the prepared silver nanoparticles solution was subjected to centrifugation for 10 min at 10000 r/min, then the obtained upper solution was stored in a refrigerator at 4°C for further use.

Instruments and Methods. 2 ml of AgNPs solution was placed in 3 ml quartz cuvette and ultraviolet and visible (UV-Vis) absorption spectra were recorded from 200 nm to 800 nm using an UH5300 UV-Vis spectrophotometer (Hitachi, Japan). TEM images were recorded on a JEM-2100F (JEOL, Japan) transmission electron microscope, TEM samples were prepared by placing a 2 μL AgNPs solution onto a copper grid (3 mm) coated with carbon film and dried with filter paper to remove excess liquid, then evaporate to dry in air. XPS characterization was performed on a PHI-5000 ESCA system (Perkin Elmer) with a monochromatic MgαK source (1253.6 eV, photon energy). HRTEM images and energy dispersive EDX were taken using a field emission gun Hitachi S-4800 (Japan) scanning electron microscope (SEM) operated at 4.0 kV. Electrochemical experiments were performed on an electrochemical workstation (CHI 660D, Chenhua Co. Ltd., Shanghai, China) with a three-electrode system with a commercial Ag/AgCl electrode as reference electrode connected with KNO_3 salt bridge, a platinum wire as the counter electrode. The electrochemical parameters of DPVs were selected as follows: potential step, 0.004 V; modulation amplitude, 50 mV; pulse width, 0.05 s; pulse period, 0.4 s. All measurements were carried out at 25°C.

Preparation and Modification of Electrodes. Firstly, a dried glass capillary (1.5 mm in diameter, 100 mm in length) was pulled on microelectrode puller. Then, a single carbon fiber (5 μm in diameter, Tokai Carbon Co., Tokai, Japan) was attached to a copper wire through silver conducting paste. After the adhesive dried, carbon fiber attached copper wire was carefully threaded into the capillary with carbon fiber exposed to the fine open end of the capillary and Cu wire exposed to the other end of the capillary. Finally, the capillary was sealed with epoxy resin with a syringe and dried

in oven at 90°C for 6 h. Prior to modification, the exposed carbon fiber was cut to a length of 0.5 mm under a microscopy. To remove possible contamination from CFME before surface modification, the prepared CFME were sequentially sonicated in acetone, 3.0 M HNO_3, 1.0 M KOH, and distilled water each for 2 min, and dried in oven.

Modification of CFME was carried out as follows. Firstly, the cleaned CFME was immersed into DMF solution containing 2 mg mL^{-1} SWNT for 5 min and dried under the infrared lamp, and the electrode was denoted as CFME/SWNT. Then, the gold nanoleaves were deposited on the CFME/SWNT electrode by applying a constant potential of - 0.2 V vs Ag/AgCl for 60 s in a 5 mM $HAuCl_4$ solution, and the electrodeposited electrode referred to CFME/SWNT/Au. Then, the CFME/SWNT/Au electrode was immersed into ethanol solution containing 50 μM SH-DNA-MB and HDT for 2 h to obtain CFME/SWNT/Au/MB+HDT electrode. After that, the CFME/SWNT/Au/MB+HDT was rinsed with ethanol and distilled water to remove the molecules of physical adsorption. Finally, CFME/SWNT/Au/MB+HDT electrode was immerged into 200 μL of AgNPs solution for 12 h, and the resulting electrode was denoted as CFME/SWNT/Au/MB+HDT/AgNPs. As a control, the corresponding electrode without SWNT (denoted as CFME/Au/MB+HDT/AgNPs), and the Au electrode modified by MB and AgNPs (denoted as Au/MB+HDT/AgNPs) was prepared to evaluate the amplification of three dimensional nanostructure of SWNTs and AuNPs.

In Vivo Experiments. All procedures involving animals were conducted strictly with acceptable ethical principles for animal research and were approved by the Animal Ethics Committees in East China Normal University. Normal mice and APPswe/PS1dE9 transgenic mice of AD (20-30 g) were supplied by Shanghai Biomodel Organism Science and Technology Development Co. Ltd. (Shanghai, China) and employed as mouse brains model of AD. Prior to animal experiments, the mouse were maintained in plastic cages with a 12 h light/dark cycle in a controlled free access to food and water for 1 month at 25°C. The age at the time of recording was 6-7 months. The surgery for mouse was performed as follows: firstly, an adult APPswe/PS1DE9 mice was anesthetized with a dose of 30 mg/100 g (i.p.) chloral hydrate, and additional doses of 10 mg/100 g (i.p.) per hour to maintain anesthesia. Then, the mouse was fixed in a stereotaxic frame (CMA Microdialysis, Kista, Sweden) with the incisor bar set at 5 mm above the interaural line and appropriately set holes drilled

through the skull. Meanwhile, a heating pad was under the mouse to keep its body temperature at 37ºC. The prepared CFME/SWNT/Au/MB+HDT/AgNPs electrode was implanted into the cortex (AP = 2.0 mm, L = 1.2 mm from the bregma, V = 1.5 mm from the surface of skull), the left striatum (AP = 0.5 mm, L = 2.0 mm anterior to the bregma, and V = 3.0 mm from the surface of skull), the dorsal hippocampus (AP = 2.3 mm, L = 2.1 mm from bregma, V =1.0 mm from the surface of the skull), respectively. An Ag/AgCl reference electrode and a counter electrode were placed into 2 cm plastic cannula with a home-made KNO_3 salt bridge, and then put it in a hole with a diameter of 0.5 mm drilled nearby the working electrode. DPV was employed for in vivo monitoring of Cl^- in mice brains.

Cerebral Ischemia Models. Adult male Wistar rats (250-300 g) were purchased from SLAC Laboratory Animal Co. (Shanghai, China), and were performed to cerebral ischemia models according to previous report.[30, 31] Briefly, the adult Wistar rat was first anesthetized and fixed on a clean platform. Then, the bilateral common carotid arteries were separated via a ventral middle line cervical incision, with special care not to damage the vagus or the sympathetic nerves running close by. Subsequently, occultation in both common carotid arteries was carried out using two Yasargil miniclips. Global ischemia duration was timed by first occluding both carotid arteries with nontraumatic arterial clips for ischemia procedure, and lasted for about 30 min.

Statistics Analysis. For all experiments, the results are expressed as mean ± SD values. $P < 0.05$ was considered as significantly different. The traditional Volhard's method for determination Cl^- was used as a standard method to evaluate the accuracy of the present electrochemical sensor. The t value was calculated according to Equation 2 and 3,

$$t = \frac{\left|\overline{x_1} - \overline{x_2}\right|}{s}\sqrt{\frac{n_1 n_2}{n_1 + n_2}} \qquad \text{(Equation 2)}$$

$$s = \sqrt{\frac{s_1^2(n_1 - 1) + s_2^2(n_2 - 1)}{(n_1 - 1) + (n_2 - 1)}} \qquad \text{(Equation 3)}$$

in which s_1 and s_2 represent the standard deviation of determined results by the present method and Volhard's method, respectively. Here n_1 and n_2 are the sample numbers of the present method and Volhard's method. If the t value is larger than standard t value, 2.78 (P = 0.05, n = 3), the result

obtained from the present method was considered is not very consistent with that obtained from Volhard's method.

ASSOCIATED CONTENT

Supporting Information

UV-Vis absorption spectra of $AgNP_S$ (Figure S1), SEM images of the modified carbon fiber microelectrodes (Figure S2), XPS data (Figure S3), the linear dependence of oxidation peak current density on scan rate (Figure S4), comparison of DPVs obtained at different modified electrodes (Figure S5), the electrode selectivity for Br^-, I^- and Cl^- (Figure S6), reproducibility test (Figure S7), stability test (Figure S8), and determination of Cl^- in the brain microdialysates by the present method and by Volhard's method (Table S1). This material is available free of charge via the internet at http://pubs.acs.org.

AUTHOR INFORMATION

Corresponding author

*Phone: +86-21-54341041; Fax: +86-21-54341041; E-mail: ytian@chem.ecnu.edu.cn.

Notes

Authors declare no competing financial interest.

ACKNOWLEDGMENTS

The authors greatly appreciate the financial support from the NSFC (21175098, 21305104, and 21635003) and the NSFC for Distinguished Young Scholars (21325521 for Y. T.). The Program of Shanghai Subject Chief Scientist (15XD1501600) and support from China Postdoctoral Science Foundation (2014M561436 and 2016T9349) are gratefully acknowledged.

REFERENCES

1. Thal, D. R., Del Tredici, K., and Braak, H. (2004) Neurodegeneration in normal brain aging and disease. *Science's SAGE KE 2004*, pe26.
2. Cardenas-Aguayo, M. a. d. C., Gomez-Virgilio, L., DeRosa, S., and Meraz-Rios, M. A. (2014) The role of tau oligomers in the onset of Alzheimer's disease neuropathology. *ACS Chem. Neurosci. 5*, 1178-1191.
3. Thal, D. R., Griffin, W. S. T., and Braak, H. (2008) Parenchymal and vascular Aβ-deposition and its effects on the degeneration of neurons and cognition in Alzheimer's disease. *J. Cell Mol. Med. 12*, 1848-1862.

4. Hardy, J., and Selkoe, D. J. (2002) The amyloid hypothesis of Alzheimer's disease: progress and problems on the road to therapeutics. *Science 297*, 353-356.
5. Jalonen, T. O., Charniga, C. J., and Wielt, D. B. (1997) β-Amyloid peptide-induced morphological changes coincide with increased K^+ and Cl^- channel activity in rat cortical astrocytes. *Brain Res. 746*, 85-97.
6. Ramírez, C. M., González, M., Díaz, M., Alonso, R., Ferrer, I., Santpere, G., Puig, B., Meyer, G., and Marin, R. (2009) VDAC and ERα interaction in caveolae from human cortex is altered in Alzheimer's disease. *Mol. Cell. Neurosci. 42*, 172-183.
7. Novarino, G., Fabrizi, C., Tonini, R., Denti, M. A., Malchiodi-Albedi, F., Lauro, G. M., Sacchetti, B., Paradisi, S., Ferroni, A., and Curmi, P. M. (2004) Involvement of the intracellular ion channel CLIC1 in microglia-mediated β-amyloid-induced neurotoxicity. *J. Neurosci. 24*, 5322-5330.
8. Paradisi, S., Matteucci, A., Fabrizi, C., Denti, M. A., Abeti, R., Breit, S. N., Malchiodi-Albedi, F., and Mazzanti, M. (2008) Blockade of chloride intracellular ion channel 1 stimulates Aβ phagocytosis. *J. Neurosci. Res. 86*, 2488-2498.
9. Correani, V., Di Francesco, L., Cera, I., Mignogna, G., Giorgi, A., Mazzanti, M., Fumagalli, L., Fabrizi, C., Maras, B., and Schininà, M. E. (2015) Reversible redox modifications in the microglial proteome challenged by beta amyloid. *Mol. BioSyst. 11*, 1584-1593.
10. Kagan, B. L., Hirakura, Y., Azimov, R., Azimova, R., and Lin, M.-C. (2002) The channel hypothesis of Alzheimer's disease: current status. *Peptides 23*, 1311-1315.
11. Mizwicki, M. T., Menegaz, D., Zhang, J., Barrientos-Durán, A., Tse, S., Cashman, J. R., Griffin, P. R., and Fiala, M. (2012) Genomic and nongenomic signaling induced by 1α, 25 $(OH)_2$-vitamin D3 promotes the recovery of amyloid-β phagocytosis by Alzheimer's disease macrophages. *J. Alzheimers Dis. 29*, 51-62.
12. D Skaper, S. (2011) Ion channels on microglia: therapeutic targets for neuroprotection. *CNS Neurolo. Disord. Drug Targets 10*, 44-56.
13. Mesquita, R. B., Fernandes, S. M., and Rangel, A. O. (2002) Turbidimetric determination of chloride in different types of water using a single sequential injection analysis system. *J. Environ. Monit. 4*, 458-461.
14. Tsikas, D., Fauler, J., and Frölich, J. (1992) Determination of chloride in biological fluids as pentafluorobenzylchloride by reversed-phase high-performance liquid chromatography and UV detection. *Chromatographia 33*, 317-320.
15. Li, P., Xie, T., Fan, N., Li, K., and Tang, B. (2012) Ratiometric fluorescence imaging for distinguishing chloride concentration between normal and ischemic ventricular myocytes. *Chem. Commun. 48*, 2077-2079.
16. Schwartz, R. D., and Yu, X. (1995) Optical imaging of intracellular chloride in living brain slices. *J. Neurosci. Meth. 62*, 185-192.
17. Inglefield, J. R., and Schwartz-Bloom, R. D. (1998) Optical imaging of hippocampal neurons with a chloride-sensitive dye: Early effects of in vitro ischemia. *J. Neurochem. 70*, 2500-2509.
18. Sah, R., and Schwartz-Bloom, R. D. (1999) Optical imaging reveals elevated intracellular chloride in hippocampal pyramidal neurons after oxidative stress. *J. Neurosci. 19*, 9209-9217.
19. Xie, X., Mistlberger, G. n., and Bakker, E. (2012) Reversible photodynamic chloride-

selective sensor based on photochromic spiropyran. *J. Am. Chem. Soc. 134*, 16929-16932.

20. Jin, J., Ouyang, X., Li, J., Jiang, J., Wang, H., Wang, Y., and Yang, R. (2011) Nucleic acid-modulated silver nanoparticles: A new electrochemical platform for sensing chloride ion. *Analyst 136*, 3629-3634.
21. Choi, H.-G., and Laibinis, P. E. (2004) Electrochemical detection of chloride by underpotentially deposited silver films on polycrystalline gold. *Anal. Chem. 76*, 5911-5917.
22. Abbas, Y., Olthuis, W., and van den Berg, A. (2013) A chronopotentiometric approach for measuring chloride ion concentration. *Sen. Actuators B-Chem. 188*, 433-439.
23. Cuartero, M., Crespo, G. n. A., and Bakker, E. (2015) Paper-based thin-layer coulometric sensor for halide determination. *Anal. Chem. 87*, 1981-1990.
24. Liu, Q., Wen, L., Xiao, K., Lu, H., Zhang, Z., Xie, G., Kong, X. Y., Bo, Z., and Jiang, L. (2016) A Biomimetic Voltage-Gated Chloride Nanochannel. *Adv. Mater. 28*, 3181-3186.
25. Alvarez-Leefmans, F. J., Gamino, S., Giraldez, F., and Nogueron, I. (1988) Intracellular chloride regulation in amphibian dorsal root ganglion neurones studied with ion-selective microelectrodes. *J. Physiol. 406*, 225-246.
26. Ashton, T. D., Jolliffe, K. A., and Pfeffer, F. M. (2015) Luminescent probes for the bioimaging of small anionic species in vitro and in vivo. *Chem. Soc. Rev. 44*, 4547-4595.
27. Han, Y., Ding, C., Zhou, J., and Tian, Y. (2015) Single Probe for Imaging and Biosensing of pH, Cu^{2+} Ions, and pH/Cu^{2+} in Live Cells with Ratiometric Fluorescence Signals. *Anal. Chem. 87*, 5333-5339.
28. Smith, B. A., Xie, B.-W., van Beek, E. R., Que, I., Blankevoort, V., Xiao, S., Cole, E. L., Hoehn, M., Kaijzel, E. L., and Löwik, C. W. (2012) Multicolor fluorescence imaging of traumatic brain injury in a cryolesion mouse model. *ACS Chem. Neurosci. 3*, 530-537.
29. Makos, M. A., Omiatek, D. M., Ewing, A. G., and Heien, M. L. (2010) Development and characterization of a voltammetric carbon-fiber microelectrode pH sensor. *Langmuir 26*, 10386-10391.
30. Zhou, J., Zhang, L., and Tian, Y. (2016) Micro Electrochemical pH Sensor Applicable for Real-Time Ratiometric Monitoring of pH Values in Rat Brains. *Anal. Chem. 88*, 2113-2118.
31. Zhao, F., Zhang, L., Zhu, A., Shi, G., and Tian, Y. (2016) In vivo monitoring of local pH values in a live rat brain based on the design of a specific electroactive molecule for H^+. *Chem. Commun. 52*, 3717-3720.
32. Luo, Y., Zhang, L., Liu, W., Yu, Y., and Tian, Y. (2015) A Single Biosensor for Evaluating the Levels of Copper Ion and L-Cysteine in a Live Rat Brain with Alzheimer's Disease. *Angew. Chem. Int. Ed. 127*, 14259-14262.
33. Cheng, H., Wang, X., and Wei, H. (2015) Ratiometric Electrochemical Sensor for Effective and Reliable Detection of Ascorbic Acid in Living Brains. *Anal. Chem. 87*, 8889-8895.
34. Xiang, L., Yu, P., Zhang, M., Hao, J., Wang, Y., Zhu, L., Dai, L., and Mao, L. (2014) Platinized Aligned Carbon Nanotube-Sheathed Carbon Fiber Microelectrodes for In Vivo Amperometric Monitoring of Oxygen. *Anal. Chem. 86*, 5017-5023.
35. Zhang, M., Yu, P., and Mao, L. (2012) Rational design of surface/interface chemistry for quantitative in vivo monitoring of brain chemistry. *Acc. Chem. Res. 45*, 533-543.
36. Kulagina, N. V., and Michael, A. C. (2003) Monitoring hydrogen peroxide in the extracellular space of the brain with amperometric microsensors. *Anal. Chem. 75*, 4875-4881.

37. Ibanez-Garcia, N., Gonçalves, R. M., da Rocha, Z. M., Gongora-Rubio, M., Seabra, A., and Chamarro, J. A. (2006) LTCC meso-analytical system for chloride ion determination in drinking waters. *Sens. Actuators, B. 118*, 67-72.
38. Hu, J., Stein, A., and Bühlmann, P. (2016) A Disposable Planar Paper-Based Potentiometric Ion-Sensing Platform. Angew. *Chem. Int. Ed. 55*, 7544-7547.
39. Painter, R. G., and Wang, G. (2006) Direct measurement of free chloride concentrations in the phagolysosomes of human neutrophils. *Anal. Chem. 78*, 3133-3137.
40. Shin, J. H., Lee, H. L., Cho, S. H., Ha, J., Nam, H., and Cha, G. S. (2004) Characterization of epoxy resin-based anion-responsive polymers: Applicability to chloride sensing in physiological samples. *Anal. Chem. 76*, 4217-4222.
41. Keighron, J. D., Wigstrom, J., Kurczy, M. E., Bergman, J., Wang, Y., and Cans, A.-S. (2015) Amperometric Detection of Single Vesicle Acetylcholine Release Events from an Artificial Cell. *ACS Chem. Neurosci. 6*, 181-188.
42. Chen, X., Parker, S. G., Zou, G., Su, W., and Zhang, Q. (2010) β-Cyclodextrin-functionalized silver nanoparticles for the naked eye detection of aromatic isomers. *ACS nano 4*, 6387-6394.
43. Kelly, K. L., Coronado, E., Zhao, L. L., and Schatz, G. C. (2003) The optical properties of metal nanoparticles: the influence of size, shape, and dielectric environment. *J. Phys. Chem. B 107*, 668-677.
44. Rai, A., Singh, A., Ahmad, A., and Sastry, M. (2006) Role of halide ions and temperature on the morphology of biologically synthesized gold nanotriangles. *Langmuir 22*, 736-741.
45. Mayagiron, J. V., Zelaya, E., Rubert, A., Benítez, G., Carro, P., Salvarezza, R. C., and Vela, M. E. (2013) Surface chemistry of 4-mercaptobenzoic acid self-assembled on Ag (111) and Ag nanoparticles. *J. Phys. Chem. C 117*, 24967-24974.
46. Du, Y., Lim, B. J., Li, B., Jiang, Y. S., Sessler, J. L., and Ellington, A. D. (2014) Reagentless, ratiometric electrochemical DNA sensors with improved robustness and reproducibility. *Anal. Chem. 86*, 8010-8016.
47. Yoo, J. J., Kim, J., and Crooks, R. M. (2015) Direct electrochemical detection of individual collisions between magnetic microbead/silver nanoparticle conjugates and a magnetized ultramicroelectrode. *Chem. Sci. 6*, 6665-6671.
48. Kato, D., Kamata, T., Kato, D., Yanagisawa, H., and Niwa, O. (2016) Au Nanoparticle-Embedded Carbon Films for Electrochemical As^{3+} Detection with High Sensitivity and Stability. *Anal. Chem. 88*, 2944-2951.
49. Tholey, G., Ledig, M., Mandel, P., Sargentini, L., Frivold, A. H., Leroy, M., Grippo, A. A., and Wedler, F. C. (1988) Concentrations of physiologically important metal ions in glial cells cultured from chick cerebral cortex. *Neurochem. Res. 13*, 45-50.
50. Enrico, P., Esposito, G., Mura, M. A., Migheli, R., Serra, P. A., Desole, M. S., Miele, E., De Natale, G., and Miele, M. (1997) Effects of allopurinol on striatal dopamine, ascorbate and uric acid during an acute morphine challenge: ex vivo and in vivo studies. *Pharmacol. Res. 35*, 577-585.
51. Van Hemelrijck, A., Sarre, S., Smolders, I., and Michotte, Y. (2005) Determination of amino acids associated with cerebral ischaemia in rat brain microdialysates using narrowbore liquid chromatography and fluorescence detection. *J. Neurosci. Meth. 144*, 63-71.
52. Amatore, C., Coffi, K., Ghandour, H., and Tong, Y. (2006) Monitoring in real time with a

microelectrode the release of reactive oxygen and nitrogen species by a single macrophage stimulated by its membrane mechanical depolarization. *Chembiochem 7*, 653-661.

53. Zielonka, J., Zielonka, M., Sikora, A., Adamus, J., Joseph, J., Hardy, M., Ouari, O., Dranka, B. P., and Kalyanaraman, B. (2012) Global profiling of reactive oxygen and nitrogen species in biological systems: high-throughput real-time analyses. *J. Biol. Chem. 287*, 2984-2995.
54. Hirokawa, T., Yoshioka, M., Okamoto, H., Timerbaev, A. R., and Blaschke, G. (2004) High-sensitivity capillary electrophoresis determination of inorganic anions in serum and urine using on-line preconcentration by transient isotachophoresis. *J. Chromatogr. B 811*, 165-170.
55. Alary, J., Bourbon, P., Escrieut, C., and Vandaele, J. (1985) Improvement of end point-detection in Volhard's method for the titration of low level of chloride ion. *Anal. Bioanal. Chem. 322*, 777-778.
56. Schwartzbloom, R. D., and Sah, R. (2001) γ-Aminobutyric $acid_A$ neurotransmission and cerebral ischemia. *J. Neurochem. 77*, 353-371.
57. Kahle, K. T., Simard, J. M., Staley, K. J., Nahed, B. V., Jones, P. S., and Sun, D. (2009) Molecular mechanisms of ischemic cerebral edema: role of electroneutral ion transport. *Physiology 24*, 257-265.
58. Eklof, B., and Siesjo, B. K. (1972) The effect of bilateral carotid artery ligation upon the blood flow and the energy state of the rat brain. *Acta Physiol. Scand. 86*, 155-165.
59. Van Hendrikse, J., Van Raamt, A. F., Der Graaf, Y. V., Der Mali, W. P. V., and Der Grond, J. V. (2005) Distribution of cerebral blood flow in the circle of Willis. *Radiology 235*, 184-189.
60. Duvernoy, H., Delon, S., and Vannson, J. L. (1981) Cortical blood vessels of the human brain. *Brain Res. Bull. 7*, 519-579.
61. Mitsos, A. P. (2015) Anatomy of the Central Nervous System (CNS) Vascular Network, In *Endovascular Neurosurgery Through Clinical Cases*, pp 11-27, Springer.

Table of Contents

Label-Free Electrochemical Biosensor for Monitoring of Chloride Ion in an Animal Model of Alzhemier's Disease

Hui Dong, Limin Zhang, Wei Liu, Yang Tian*

Shanghai Key Laboratory of Green Chemistry and Chemical Processes, Department of Chemistry, School of Chemistry and Molecular Engineering, East China Normal University, Dongchuan Road 500, Shanghai 200241, China.